

## THE ORIGIN OF THE YOUNG STARS IN THE NUCLEUS OF M31

PHILIP CHANG<sup>1,2</sup>, RUTH MURRAY-CLAY<sup>1</sup>, EUGENE CHIANG<sup>1</sup>, & ELIOT QUATAERT<sup>1</sup>

*Draft version February 24, 2019*

### ABSTRACT

The triple nucleus of M31 consists of a population of old red stars in an eccentric disk (P1 and P2) and another population of younger A stars in a circular disk (P3) around M31’s central supermassive black hole (SMBH). We argue that P1 and P2 determine the maximal radial extent of the younger A star population and provide the gas that fueled the starburst that generated P3. The eccentric stellar disk creates an  $m = 1$  non-axisymmetric perturbation to the potential. This perturbed potential drives gas into the inner parsec around the SMBH, if the pattern speed of the eccentric stellar disk is  $\Omega_p \lesssim 3 - 10 \text{ km s}^{-1} \text{ pc}^{-1}$ . We show that stellar mass loss from P1 and P2 is sufficient to create a gravitationally unstable gaseous disk of  $\sim 10^5 M_\odot$  every 0.1 – 1 Gyrs, consistent with the 200 Myr age of P3. Similar processes may act in other systems to produce very compact nuclear starbursts.

*Subject headings:* galaxies: individual (M31) – galaxies: nuclei – galaxies: starburst

### 1. INTRODUCTION

In balloon-borne experiments, Light et al. (1974) discovered that the nucleus of M31 is asymmetric. Observations with the Hubble Space Telescope (HST) resolved the nucleus into two components (Lauer et al. 1993). The two nuclei, denoted P1 and P2, have an angular separation of  $0''.5$  ( $\approx 2$  pc at the distance of M31; Bender et al. 2005, hereafter B05). P2 is located near the dynamical center while P1, the brighter nucleus, is offset. P1 and P2 have a total luminosity of  $\approx 3 \times 10^6 L_\odot$ . For a mass-to-light ratio of 5.7 appropriate for a bulge population (Tremaine 1995, hereafter T95), the total stellar mass is  $\approx 2 \times 10^7 M_\odot$ .

P1 and P2 are unlikely to be separate stellar clusters because the time for dynamical friction to merge such clusters would be short ( $\sim 10^6$  yrs if P1 is a  $\sim 10^7 M_\odot$  cluster; T95). Instead, P1 and P2 are best modeled as a single eccentric stellar disk, as originally proposed by T95 (see also Peiris & Tremaine 2003, hereafter PT03). Disk stars slow near apocenter, giving rise to P1. Stars near pericenter give rise to P2. The central supermassive black hole (SMBH) sits within P2.

Spectroscopically, P1 and P2 are nearly identical, consistent with the eccentric stellar disk model. However, P2 is bluer. Neito et al. (1986) showed that P2 is brighter than P1 at 3750 Å. King et al. (1995) showed that P2 is brighter than P1 in the ultraviolet. Though this difference was initially attributed to an active galactic nucleus (AGN), recent HST spectroscopy of the nuclear region of M31 has uncovered a younger population of 200-Myr old A stars, embedded in P2 (B05). This population, named P3, appears to be a disk of stars with a mass of  $\sim 4200 M_\odot$  and a maximal radial extent of  $\approx 1$  pc (B05; Bender priv. communication) that surrounds the central SMBH and lies in the same plane as the P1/P2 disk. Using the line-of-sight velocities ( $\approx 1000 \text{ km s}^{-1}$ ) measured for P3, B05 estimate that the mass of the SMBH in M31

is  $1.1 - 2.1 \times 10^8 M_\odot$ .

P3 is a stellar population distinct from P1 and P2 (B05). P3 is composed of A stars while P1 and P2 are typical old red bulge stars. The relative youth of these A stars and their proximity to the central SMBH make P3 analogous to the young stars in our Galactic Center (GC). Like the young stars in the GC, P3 must either form in situ or migrate in from larger radii. Migration is less likely in M31 than in the GC as the progenitor cluster would be disrupted at greater distances from the more massive SMBH in M31. In situ formation more naturally explains the masses of these central star-forming regions through Toomre stability arguments (see § 3). However, it is less clear what sets the radial extents ( $r \lesssim 1$  pc for M31;  $r \lesssim 0.4$  pc for the GC) and ages ( $\approx 200$  Myr for M31;  $\approx 10$  Myr for the GC) of these nuclear starbursts.

In this paper, we address these questions by demonstrating that the eccentric stellar disk of M31 fixes both the radial extent and the timescale for the starburst that generated P3. In § 2, we argue that the non-axisymmetric potential from the eccentric stellar disk limits non-intersecting gas orbits to a limited family around the central SMBH. The physics is similar to what sets the maximum sizes of accretion disks in Roche-lobe filling binaries (Paczynski 1977; Papaloizou & Pringle 1977). We present numerical and analytic calculations describing how non-intersecting gas orbits are only allowed for  $r \lesssim 1$  pc if the pattern speed of the P1/P2 disk is  $\lesssim 3 - 10 \text{ km s}^{-1} \text{ pc}^{-1}$ . This naturally explains the size of P3. We then argue in § 3 that stellar mass loss from the P1/P2 disk is sufficient to supply the gas needed to form P3. We estimate the mass required to trigger a starburst and the timescale to build up that mass, and show that these are consistent with the mass and age of P3. Finally, we conclude in § 4, drawing attention to a few predictions of our model and arguing that this mechanism may be common in galactic nuclei.

### 2. CLOSED GAS ORBITS IN AN ECCENTRIC STELLAR DISK

In the limit that gas has zero pressure, gas follows test particle orbits that are simply closed and non-crossing (Paczynski 1977). Gas not in these orbits will shock

<sup>1</sup> Astronomy Department and Theoretical Astrophysics Center, 601 Campbell Hall, University of California, Berkeley, CA 94720; pchang@astro.berkeley.edu, rmurray@astro.berkeley.edu, echiang@astro.berkeley.edu, eliot@astro.berkeley.edu

<sup>2</sup> Miller Institute for Basic Research

against gas in neighboring orbits (i.e., crossing) or itself (i.e., not simply closed). These shocks dissipate orbital energy, driving gas to lower energy orbits. Paczynski (1977) applied this principle to solve for the maximum size of a gaseous accretion disk in a Roche-filling binary star system. Test particle orbits that are close to the accretor, where the potential is nearly Keplerian, can be nearly circular and non-crossing. Farther from the accretor, the non-axisymmetric component of the potential (due to the donor star) becomes larger until test particle orbits are forced to cross either their neighbors or themselves. Therefore there exists a maximum radius for gas orbits in the vicinity of the accretor: the tidal truncation radius,  $R_t$  (Papaloizou & Pringle 1977). Gas outside  $R_t$  will be driven toward it through dissipative processes, while gas inside  $R_t$  will occupy the allowed orbits, forming a gaseous accretion disk. Paczynski (1977) showed that only one family of orbits is possible for any given binary system with a specified mass ratio. These results were later confirmed by numerical simulations of close binary systems by Ichikawa & Osaki (1994).

By analogy, P1 and P2 add a non-axisymmetric component to the point mass potential of the central SMBH in M31. Thus, there should also be an  $R_t$  inside of which a gaseous accretion disk can exist around the SMBH. While this situation is similar to that of a close binary star system, there are two differences. First, the perturbation to the potential in M31 is given by the eccentric stellar disk. Second, whereas the pattern speed of the perturbation potential in a binary star system is prescribed by the binary orbital frequency, the pattern speed of the P1/P2 disk (i.e., its apsidal precession frequency) is uncertain (see Appendix A for estimates in the literature).

Since the gas mass required to form P3 ( $M_{\text{gas}} \lesssim 10^5 M_\odot$ ; see § 3) is much smaller than the mass of the P1/P2 disk and the central SMBH, and since we assume that Toomre's  $Q > 1$  for the present discussion (§ 3), we neglect gas self-gravity. Moreover, since the characteristic temperature of the gas is  $T \sim 30$  K (§ 3), the thermal energy of a gas particle,  $\sim kT$ , where  $k$  is Boltzmann's constant, is much smaller than the particle's gravitational energy due to the P1/P2 disk,  $\sim GM_D \mu / R_D$ . Here  $G$  is the gravitational constant,  $M_D \approx 2 \times 10^7 M_\odot$  and  $R_D \sim 1$  pc are the mass and characteristic size of the disk, respectively, and  $\mu$  is the mean molecular weight of the gas. Therefore, as Paczynski (1977) originally envisioned, gas orbits can be computed in the zero pressure limit.

To calculate  $R_t$ , we look for simply closed and non-crossing orbits in the combined potential of a central SMBH and an eccentric, precessing stellar disk. All orbits are computed in the  $(x, y)$  plane of the eccentric stellar disk. We orient P1 and P2 such that P1 is centered at  $x = -3$  pc (which corresponds to the 2 pc separation projected on the sky). The SMBH is fixed at the origin. We assume that the P1/P2 disk precesses rigidly counterclockwise with pattern speed  $\Omega_p$  about the center of mass, located at  $(x_{\text{cm}}, 0)$ . In the rotating frame, the equations of motion are

$$\ddot{x} = -\frac{d\Phi}{dx} + \Omega_p^2 (x - x_{\text{cm}}) + 2\Omega_p \dot{y} \quad (1)$$

$$\ddot{y} = -\frac{d\Phi}{dy} + \Omega_p^2 y - 2\Omega_p \dot{x}, \quad (2)$$

where the potential  $\Phi$  is given by

$$\Phi(x, y) = -\frac{GM_{\text{BH}}}{r} + \Phi_D(x, y), \quad (3)$$

where  $M_{\text{BH}}$  is the mass of the central SMBH,  $r = \sqrt{x^2 + y^2}$ , and  $\Phi_D$  is the potential due to the eccentric disk:

$$\Phi_D(x, y) = -G \int dx' dy' \frac{\Sigma(x', y')}{|r - r'| + h} \quad (4)$$

where  $|r - r'| = \sqrt{(x - x')^2 + (y - y')^2}$ ,  $\Sigma$  is the stellar mass surface density, and  $h$  is the softening length to account for the finite thickness of the disk. For now, we take a fixed softening length of  $h = 0.1$  pc to cleanly demonstrate how the P1/P2 disk can tidally truncate a gaseous disk. The P1/P2 disk may be substantially thicker, however. At the end of this section, we discuss various choices for  $h$  and their effects on our results.

For  $\Sigma$ , we use the fit to the light distribution from PT03 and a mass-to-light ratio of 5.7 (T95; PT03). We focus on PT03's non-aligned model as it fits the light distribution and kinematic data better for P1 and P2. In addition, we ignore the contribution to the potential from the local bulge because its mass is only 10% of that of the disk ( $\lesssim 10^6 M_\odot$ ; PT03). We refer the interested reader to Appendix A for more details.

The strength of the non-axisymmetric component relative to the axisymmetric component depends on the mass of the P1/P2 disk relative to that of the SMBH,  $M_D/M_{\text{BH}}$ . PT03 give a stellar mass of  $\approx 2 \times 10^7 M_\odot$  for a mass-to-light ratio appropriate for the bulge and fit a SMBH mass of  $10^8 M_\odot$ . Salow & Statler (2001, 2004) construct a series of self-consistent dynamical models, which give stellar masses of  $1 - 2 \times 10^7 M_\odot$  and a SMBH mass of  $\approx 5 \times 10^7 M_\odot$ . B05 give a SMBH mass of  $1.4 \times 10^8 M_\odot$  ( $1.1 - 2.1 \times 10^8 M_\odot$  at the  $1\sigma$  error level) based on the dynamics of P3. The range of mass ratios,  $M_D/M_{\text{BH}}$ , from these different authors is  $\approx 0.1 - 0.3$ . We adopt a fiducial ratio of  $M_D/M_{\text{BH}} = 0.1$  motivated by the stellar disk mass from PT03 and the SMBH mass from B05; in this case  $x_{\text{cm}} = -0.07$  pc.

We compute test particle (gas) orbits using equations (1) and (2). The orbit starts at  $x = -R_1$  with a velocity purely in the  $-y$  direction ( $\dot{x} = 0$ ); see Figure 1. Stars rotate about the SMBH in the counterclockwise direction. We take the gas rotation and the P1/P2 disk pattern speed to also be in the counterclockwise directions. For each computed orbit, we check to see if the ending position and velocity are the same as the beginning position and velocity. We vary the initial velocity  $\dot{y}$  until this condition is met. We define  $R_2$  as the position where the orbit crosses the positive  $x$ -axis. Repeating this calculation over a range of  $R_1$ , we find a family of simply closed orbits for a given pattern speed  $\Omega_p$ .

Figure 1 shows such simply closed orbits for  $M_D/M_{\text{BH}} = 0.1$ ,  $M_{\text{BH}} = 10^8 M_\odot$ , and  $\Omega_p = 3 \text{ km s}^{-1} \text{ pc}^{-1}$ . At such a low pattern speed, gas orbits are restricted to lie inside a maximal orbit (thick solid line), which we denote the  $R_t$  orbit. Gas outside this orbit will cross the  $R_t$  orbit (as in the outermost two orbits in Fig. 1) or be self-crossing.

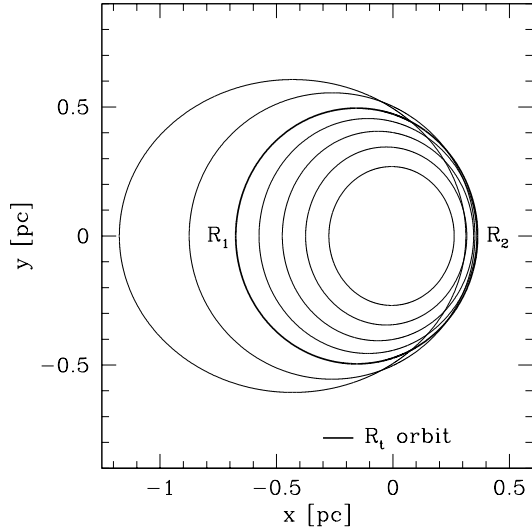


FIG. 1.— Gas orbits for  $\Omega_p = 3 \text{ km s}^{-1} \text{ pc}^{-1}$ ,  $M_{\text{BH}} = 10^8 M_{\odot}$ ,  $M_D/M_{\text{BH}} = 0.1$ , and a softening length of  $h = 0.1 \text{ pc}$ . The largest possible orbit, denoted  $R_t$ , is shown with the thick solid line. The outermost two orbits have their closest approach inside of the  $R_t$  orbit (they also cross each other). Gas in orbits exterior to the  $R_t$  orbit will shock and be driven to it. Note that the  $R_t$  orbit is very eccentric.

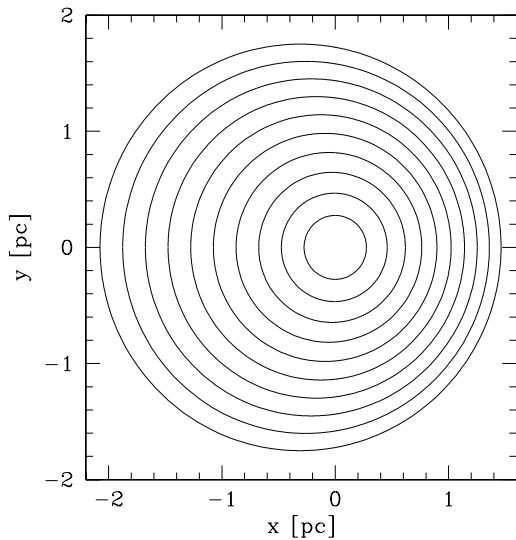


FIG. 2.— Same as Figure 1, except  $\Omega_p = 30 \text{ km s}^{-1} \text{ pc}^{-1}$ . Unlike in Figure 1, there is no  $R_t$  orbit. Gas finds non-crossing orbits at all radii.

Figure 2 shows orbits for a higher pattern speed  $\Omega_p = 30 \text{ km s}^{-1} \text{ pc}^{-1}$ . These orbits form non-crossing orbits spanning the entire disk. Figures 1 and 2 illustrate that the nature of gas orbits qualitatively changes when going from low to high pattern speeds. Gas occupies restricted orbits at low pattern speeds, while at higher pattern speeds, gas can span the entire disk.

We plot  $R_2$  as a function of  $R_1$  for different values of  $\Omega_p$  in Figure 3. For small  $\Omega_p$ ,  $R_2$  has a local maximum,  $R_{2,\text{max}}$  (marked with solid black squares in Fig. 3). We denote the  $R_1$  for which this occurs as  $R_{1,\text{max}}$ . Beyond  $R_1 \approx 3 \text{ pc}$ ,  $R_2$  increases with  $R_1$  for all  $\Omega_p$ .

We define the tidal truncation radius as the angle-

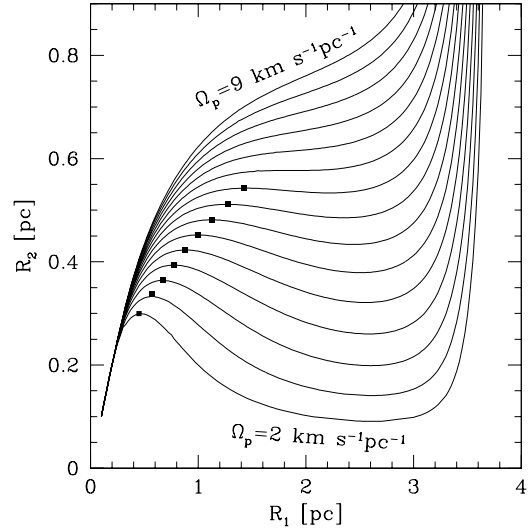


FIG. 3.—  $R_2$  (periapse distance) as a function of  $R_1$  (apoapse distance) for  $\Omega_p = 2 - 9 \text{ km s}^{-1} \text{ pc}^{-1}$  in  $0.5 \text{ km s}^{-1} \text{ pc}^{-1}$  intervals, for  $M_D/M_{\text{BH}} = 0.1$ ,  $M_{\text{BH}} = 10^8 M_{\odot}$ , and  $h = 0.1 \text{ pc}$ . For small  $\Omega_p$ ,  $R_2$  obtains a local maximum, which we mark with a solid black square. For  $\Omega_p > 6 \text{ km s}^{-1} \text{ pc}^{-1}$ , this local maximum does not exist.

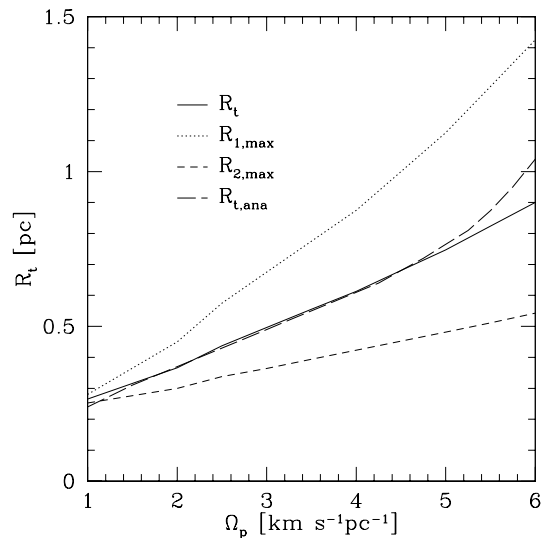


FIG. 4.—  $R_t$  (solid line) as a function of  $\Omega_p$  for  $M_D/M_{\text{BH}} = 0.1$ ,  $M_{\text{BH}} = 10^8 M_{\odot}$ , and  $h = 0.1 \text{ pc}$ . We also plot  $R_{1,\text{max}}$  (dotted line),  $R_{2,\text{max}}$  (short dashed line), and  $R_{t,\text{ana}}$  (long dashed line) as defined by the crossing condition (eq.[8]). For  $\Omega_p \gtrsim 6 \text{ km s}^{-1} \text{ pc}^{-1}$ , gas orbits can persist at all radii.

averaged radius of the maximal non-intersecting orbit:  $R_t = (2\pi)^{-1} \int R(\theta) d\theta$ . Figure 4 shows  $R_t$  as a function of  $\Omega_p$ . As  $\Omega_p$  increases,  $R_t$  increases. The tidal truncation radius,  $R_t$ , is  $\lesssim 1 \text{ pc}$  (similar to the observed maximal radial extent of P3) when  $\Omega_p \lesssim 6 \text{ km s}^{-1} \text{ pc}^{-1}$  for  $M_D/M_{\text{BH}} = 0.1$  and  $M_{\text{BH}} = 10^8 M_{\odot}$ . For larger pattern speeds,  $R_t$  does not exist and a gaseous disk can span all radii.

The dependence of  $R_t$  on  $\Omega_p$ ,  $M_D$ , and  $M_{\text{BH}}$  can be derived using perturbation theory (e.g., Papaloizou & Pringle 1977; Binney & Tremaine 1987). In cylindrical

coordinates  $(r, \phi)$ , the equations of motion in the frame rotating at  $\Omega_p$  are

$$\ddot{r} = -\frac{d\Phi}{dr} + \frac{l^2}{r^3} + \frac{2\Omega_p l}{r} + \Omega_p^2 r \quad (5)$$

$$\dot{l} = -\frac{d\Phi}{d\phi} - 2\Omega_p r \dot{r}, \quad (6)$$

where  $l = r^2 \dot{\phi}$  is the specific angular momentum.<sup>3</sup> Following the derivation in Binney & Tremaine (1987), we take  $\Phi \rightarrow \Phi_0(r) + \sum_{m=1}^{\infty} \Phi_m(r, \phi)$ ,  $r \rightarrow r + \delta r$  and  $\phi \rightarrow \phi + \delta\phi$  in the epicyclic approximation, where  $\Phi_m = \Phi_{m,0}(r) \cos[m(\Omega - \Omega_p)t]$  are the Fourier components of the potential and  $\Omega = \sqrt{r^{-1}d\Phi_0/dr}$  is the orbital frequency at the guiding center,  $r$ . If the axisymmetric component ( $\Phi_0$ ) is dominant, the solution for  $\delta r$  is (Binney & Tremaine 1987, their eq.[3.119ab])

$$\delta r = -\frac{\cos(m(\Omega - \Omega_p)t)}{\kappa^2 - m^2(\Omega - \Omega_p)^2} \left( \frac{d\Phi_{m,0}(r)}{dr} + \frac{2\Omega\Phi_{m,0}(r)}{(\Omega - \Omega_p)r} \right) + C \cos(\kappa t + \psi), \quad (7)$$

where  $\kappa^2 = d^2\Phi_0/dr^2 + 3\Omega^2$  is the square of the epicyclic frequency,  $C$  and  $\psi$  are constants, and we assume that the perturbation is dominated by a single mode  $m$ . Note that simply closed orbits correspond to  $C = 0$ . For the eccentric stellar disk, the dominant Fourier mode is  $m = 1$ , whose amplitude we numerically calculate and plot in Figure 5.

Orbits first cross their neighbors at pericenter (i.e.,  $\delta r < 0$ ; see Figure 1) when

$$\frac{d\delta r}{dr} < -1; \quad (8)$$

i.e., when the epicyclic amplitude grows faster than the size of the guiding center orbit (Papaloizou and Pringle 1977). From our numerically calculated  $\Phi_{1,0}$ , we evaluate  $d\delta r/dr$  as a function of  $r$  and determine an analytic tidal truncation radius,  $R_{t,ana}$ , where  $d\delta r/dr$  first equals  $-1$ . We plot  $R_{t,ana}$  in Figure 4 to compare to the numerically calculated  $R_t$ . The agreement is good.

Since the potential is nearly Keplerian ( $\kappa \approx \Omega$ ) and since  $\Omega_p/\Omega \ll 1$ , we expand equation (7) to first order in  $\Omega_p/\Omega$  and  $\Phi_1/\Phi_0$ . For  $d/dr \sim 1/r$ , the condition for first orbit crossing (eq.[8]) becomes

$$\frac{|\delta r|}{r} \sim \frac{\Omega}{\Omega_p} \frac{\Phi_1}{\Phi_0} \sim 1, \quad (9)$$

where we drop numerical factors. Equation (9) indicates that for the fixed  $R_t$  orbit,  $\Omega_p \propto \Omega\Phi_1/\Phi_0$ . Since  $\Phi_1/\Phi_0$  scales as  $M_D/M_{BH}$  and  $\Omega$  scales as  $M_{BH}^{1/2}$ , we find:

$$\Omega_p \propto M_{BH}^{-1/2} M_D. \quad (10)$$

We demonstrated earlier (see Figure 4) that gas orbits are limited to an inner disk similar to the maximal radial extent of P3 (i.e.,  $R_t < 1$  pc) if the pattern speed  $\Omega_p \lesssim 6 \text{ km s}^{-1} \text{ pc}^{-1}$  for  $M_{BH} = 10^8 M_\odot$  and  $M_D/M_{BH} = 0.1$ .

<sup>3</sup> We assume in the following that the disk precession axis passes through the origin (SMBH).

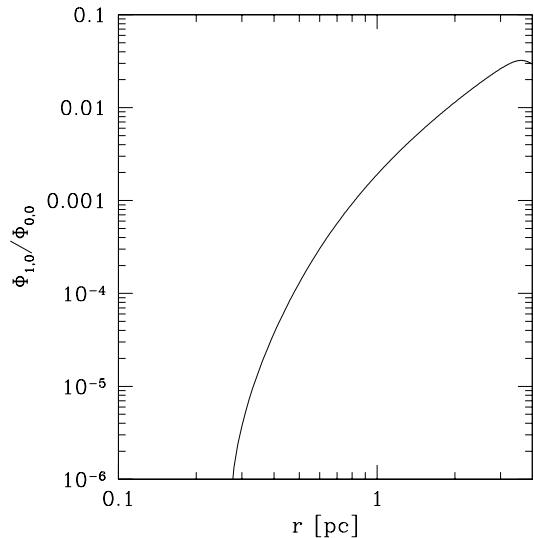


FIG. 5.— Ratio of  $\Phi_{1,0}$  ( $m = 1$  component of the potential) to  $\Phi_{0,0}$  (axisymmetric component of the potential) as a function of  $r$  for  $M_D/M_{BH} = 0.1$ .

Inserting the scalings from (10), we rescale this pattern speed to be

$$\Omega_p \lesssim 6 \left( \frac{M_{BH}}{10^8 M_\odot} \right)^{-1/2} \left( \frac{M_D}{10^7 M_\odot} \right) \text{ km s}^{-1} \text{ pc}^{-1}. \quad (11)$$

We have confirmed these scalings numerically. For M31, if  $M_D \approx 2 \times 10^7 M_\odot$  (PT03) and  $M_{BH} \approx 1.4 \times 10^8 M_\odot$  (B05), then equation (11) gives  $\Omega_p \lesssim 10 \text{ km s}^{-1} \text{ pc}^{-1}$ .

We now return to the issue of the thickness of the P1/P2 disk and its impact on  $R_t$ . The non-aligned model of PT03, which we use for the surface density profile, uses  $h/r \approx 0.4$ . On the other hand, the disk models of Salow and Statler (2001, 2004) are razor thin. Bacon et al. (2001) also advocate a cold thin disk ( $h/r \sim 0.1$ ) to model P1 and P2. Toomre stability arguments give a minimum  $h/r$  of  $\approx 0.1$  (PT03; see also Bacon et al. 2001). If the P1/P2 disk has persists for  $10^{10}$  years, two-body relaxation gives a minimum  $h/r \approx 0.2$  (PT03; T95).

How does varying the softening length affect our results? In Figure 6, we plot  $R_t$  as a function of  $\Omega_p$  for various softening parameters of  $h/r = 0.1 - 0.4$ , taking  $M_D = 2 \times 10^7 M_\odot$  and  $M_{BH} = 1.4 \times 10^8 M_\odot$  as is appropriate for M31. The results for  $h = 0.1$  pc, which we have focused on thus far, differ from those for  $h/r = 0.1$  by  $\approx 10\%$ . However, as Figure 6 shows, thicker disks show more substantial differences. As we increase the softening parameter from  $h/r = 0.1$  to  $0.4$ , the maximum  $\Omega_p$  for which  $R_t$  exists decreases, down to  $\approx 2 \text{ km s}^{-1} \text{ pc}^{-1}$ . In addition, the maximum  $R_t$  also decreases, down to  $\approx 0.4$  pc. To produce  $R_t \lesssim 1$  pc, similar to the observed maximal radius ( $\sim 1$  pc) of the P3 disk (B05), we require  $\Omega_p \lesssim 3 - 10 \text{ km s}^{-1} \text{ pc}^{-1}$  for  $h/r = 0.1 - 0.3$ .

Finally, we estimate the time,  $t_{flow}$ , for gas to flow to  $R_t$  from larger radii. Compared to the axisymmetric component of the potential, the  $m = 1$  component is smaller by of order  $10^{-3} - 10^{-2}$  for  $r \gtrsim 1$  pc (see Fig. 5). We expect the epicyclic velocity to be  $\delta v \sim \sqrt{\Phi_1/\Phi_0} v_{orb} \approx 0.1 v_{orb} \approx 70 \text{ km s}^{-1}$  at 1 pc, where  $v_{orb}$  is the orbital ve-

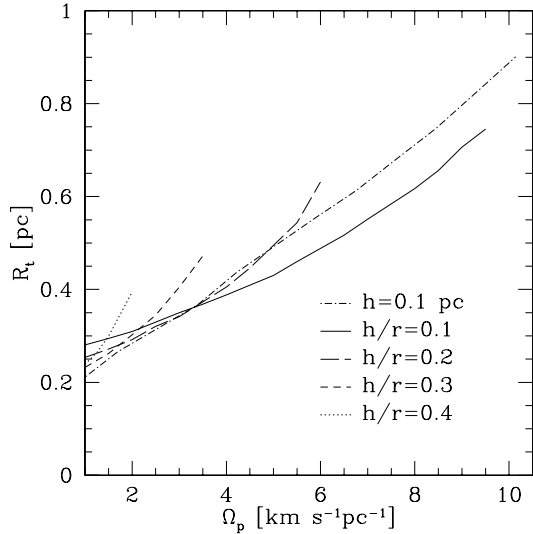


FIG. 6.—  $R_t$  as a function of  $\Omega_p$  for parameters appropriate to M31 ( $M_D = 2 \times 10^7 M_\odot$  and  $M_{\text{BH}} = 1.4 \times 10^8 M_\odot$ ) for various softening parameters of  $h/r = 0.1$  (solid line), 0.2 (long-dashed line), 0.3 (short-dashed line), and 0.4 (dotted line). We also show the softening length,  $h = 0.1$  pc, (dashed-dotted line) for comparison.

locity. This is much greater than the gas sound speed,  $c_s \sim 0.3 - 1 \text{ km s}^{-1}$  at  $T \sim 10 - 100 \text{ K}$ . Gas streams cross at supersonic velocities, shock, and dissipate  $\Phi_1/\Phi_0$  of their orbital energy per dynamical time,  $t_{\text{dyn}} = \Omega^{-1}$ . Thus the inflow time  $t_{\text{flow}} \sim t_{\text{dyn}} (\Phi_1/\Phi_0)^{-1}$ , which is a few hundred to a few thousand dynamical times. At  $r \sim 1 \text{ pc}$ ,  $t_{\text{flow}} \sim 10^5 - 10^6 \text{ yrs}$ .

### 3. STELLAR MASS LOSS AS THE ORIGIN OF THE GAS THAT FORMED P3

In § 2 we argued that gas at  $r \gtrsim R_t$  is forced down to  $r \approx R_t$  on short timescales,  $t_{\text{flow}} \sim 10^6 \text{ yrs}$ . Supplied with sufficient mass, the gas disk at  $\approx R_t$  eventually becomes gravitationally unstable, forming stars and giving rise to P3. We now explore these questions of gas supply and gravitational instability.

There are a number of potential sources of gas. For example, molecular clouds can be gravitationally scattered onto low angular momentum orbits. The rate of such gas supply is difficult to quantify, however. Here we focus instead on mass supply due to winds from stars in the P1/P2 disk. This source of mass is unavoidable, existing even in the absence of external sources. We show below that mass loss from the P1/P2 disk is sufficient to trigger a starburst having the right properties to explain P3.

The P1/P2 disk consists of  $\approx 2 \times 10^7 M_\odot$  of stars with an age of  $\sim 10^{10} \text{ yrs}$  (B05, PT03). We compute the stellar mass loss rate from Starburst99 (Leitherer et al. 1999; Vazquez & Leitherer 2005), using the Padova tracks with asymptotic giant branch (AGB) stars. A  $\sim 10^{10} \text{ yr}$  old star cluster of mass  $2 \times 10^7 M_\odot$  loses mass via stellar winds at a rate  $\dot{M}_* \approx 3 \times 10^{-5} - 3 \times 10^{-4} M_\odot \text{ yr}^{-1}$ . The mass loss is primarily due to winds from red giants and thermally pulsating AGB stars. There are uncertainties in these mass loss rates due to uncertainties in the properties of the thermally pulsating AGB

stars. The stellar winds which dominate the mass loss have velocities ( $5 - 25 \text{ km s}^{-1}$  for AGB stars; Lamers & Cassinelli 1999) much lower than the orbital velocity  $v_{\text{orb}} \sim 700 \text{ km s}^{-1}$ . Hence the winds are bound to the nuclear region. The winds have typical relative velocities of  $\sim (h/r)v_{\text{orb}} \sim 200 \text{ km s}^{-1}$ , where  $h \sim 0.3r$  is the thickness of the P1/P2 disk. The stellar winds thus shock, reaching temperatures of  $\sim 10^6 [(h/r)/0.3]^2 \text{ K}$ . The fate of the shocked stellar wind material depends on the competition between heating and cooling. For rapid cooling, the gas will collapse to form a thin disk. For slow cooling, it will heat up because of viscous stresses and form a geometrically thick, radiatively inefficient accretion flow. The gas heats up on a characteristic timescale  $t_{\text{heat}} \approx \alpha^{-1} \Omega^{-1}$ , where  $\alpha$  is the dimensionless viscosity.<sup>4</sup> The cooling time is given by  $t_{\text{cool}} \approx 3kT/2n\Lambda(T)$  where  $\Lambda(T)$  is the cooling function for an optically thin thermal plasma. The density of stellar wind material that accumulates on a timescale  $t_{\text{heat}}$  is  $n \approx \dot{M}_* t_{\text{heat}} / (2\pi r^3 [h/r] \mu)$ . If  $t_{\text{cool}} \lesssim t_{\text{heat}}$  for gas at this density, it will cool and collapse to form a thin disk. This condition can be written as a constraint on the stellar wind mass loss rate

$$\dot{M}_* \gtrsim \dot{M}_{*,\text{crit}} \approx \frac{3\pi r \alpha^2 [h/r]^3 \mu^2 v_{\text{orb}}^4}{5\Lambda(T)}. \quad (12)$$

Taking  $\alpha = 0.1$ ,  $M_{\text{BH}} = 10^8 M_\odot$  and  $r = 2 \text{ pc}$  as fiducial numbers for M31, we find that  $\dot{M}_{*,\text{crit}} \approx 4 \times 10^{-7} - 6 \times 10^{-6} M_\odot \text{ yr}^{-1}$  for  $h/r = 0.2 - 0.4$ . Since  $\dot{M}_* \approx 3 \times 10^{-5} - 3 \times 10^{-4} M_\odot \text{ yr}^{-1}$  for the stars in the P1/P2 disk, we conclude that stellar winds from P1/P2 will likely cool and collect in a geometrically thin disk.<sup>5</sup>

Cooled gas accumulates at  $R_t \sim 1 \text{ pc}$  until it either accretes onto the SMBH or becomes gravitationally unstable and fragments into stars (see related arguments of Nayakshin 2006 and Levin 2007). For a disk to fragment into stars, numerical studies suggest that two conditions must be met (Gammie 2001; see also Shlosman & Begelman 1989):

$$Q \lesssim 1, \quad (13)$$

$$t_{\text{cool}} \lesssim 3t_{\text{dyn}}, \quad (14)$$

where  $Q = c_s \kappa / \pi G \Sigma_g$  is the Toomre parameter,  $c_s = \sqrt{kT/\mu}$  is the gas sound speed,  $\Sigma_g$  is the gas surface density of the disk, and  $t_{\text{dyn}} = \Omega^{-1}$  is the local dynamical time. The radiative cooling time,  $t_{\text{cool}}$ , is given by

$$\frac{\Sigma_g kT}{\mu t_{\text{cool}}} \sim \sigma_B T^4 \begin{cases} \tau_{\text{IR}} & \tau_{\text{IR}} \ll 1 \\ \tau_{\text{IR}}^{-1} & \tau_{\text{IR}} \gg 1 \end{cases}, \quad (15)$$

where  $\tau_{\text{IR}} = \kappa_{\text{IR}} \Sigma_g / 2$  is the infrared (IR) vertical optical depth of the gas disk,  $T$  is the midplane temperature of the disk, and  $\kappa_{\text{IR}}$  is the corresponding opacity. The first condition (eq. [13]) is that gas self-gravity must overcome rotation and gas pressure. The second condition

<sup>4</sup> The heating from the gravitational torques exerted by the eccentric stellar disk is small compared to that from  $\alpha$ -viscosity for an initially thick disk.

<sup>5</sup> Our critical  $\dot{M}_{*,\text{crit}}$  is a factor of  $\gtrsim 20$  smaller than that usually estimated for the transition from a thin to thick disk (e.g., Fig. 3 of Menou, Narayan, & Lasota 1999). The latter calculations assume  $h \approx r$ , i.e., that a thick disk is already established, while in our problem the stellar winds are initially confined to a region with  $h \approx 0.3r$ . Smaller  $h/r$  increases  $n$  and decreases  $T$  at fixed  $\dot{M}_*$ , thus significantly decreasing the cooling time of the gas.

(eq. [14]) is that cooling is sufficiently rapid to overcome heating due to gravitationally induced turbulence (“gravitoturbulence”; e.g., Shlosman et al. 1989; Gammie 2001). If equation (13) is satisfied, but equation (14) is not, then the disk enters a gravitoturbulent state and accretes, but does not fragment or form stars.

The ability of the gas disk to fragment into stars thus depends on the heating and cooling of the gas. We consider two possibilities for the heating: external heating by stellar irradiation from the P1/P2 disk and intrinsic heating by gravitoturbulence. We take the gas to cool radiatively by emission from dust grains.<sup>6</sup> When the gas is externally heated by starlight,  $Q > 1$  initially for a sufficiently low mass disk. The disk mass grows from stellar winds until  $Q \sim 1$ , when it becomes gravitationally unstable. If equation (14) is also satisfied, then the disk fragments.

When external sources of heat are negligible, gravitoturbulence tends to maintain the disk in a marginally stable state with  $Q \sim 1$  (Gammie 2001). Initially, the disk does not fragment because the cooling time is long under these conditions. As the mass in the disk increases from stellar winds, the cooling time decreases relative to the orbital period, and eventually fragmentation occurs. Whether the gas is heated by starlight or by gravitoturbulence, fragmentation is a function of  $M_{\text{gas}}$  (see also Nayakshin 2006 and Levin 2007).

We first consider stellar irradiation, which is dominated by the P1/P2 disk. The stars in the P1/P2 disk are on average  $R_D \sim 1 - 3$  pc from any patch of the gaseous disk, whose vertical thickness is  $\ll h$ , the thickness of the stellar disk. For the purposes of this section, we will adopt fiducial values of  $R_D \sim 2$  pc and  $h/R_D \sim 0.3$  motivated by our previous discussion in § 2. The flux of starlight incident on the disk is  $F_* \sim (L_*/4\pi R_D^2)(h/R_D) \approx 10(L_*/3 \times 10^6 L_\odot)(R_D/2 \text{ pc})^{-2}([h/R_D]/0.3) \text{ ergs cm}^{-2} \text{ s}^{-1}$ , where  $L_*$  is the total stellar luminosity of the P1/P2 disk. The disk is easily optically thick to incident starlight for typical optical opacities (for dust-to-gas ratios of 0.01; Draine 2003). We define the effective temperature from starlight heating as

$$\sigma T_{e,*}^4 = F_* = \frac{L_*}{4\pi R_D^2} \frac{h}{R_D}, \quad (16)$$

which gives

$$T_{e,*} \approx 20 \left( \frac{L_*}{3 \times 10^6 L_\odot} \right)^{1/4} \left( \frac{R_D}{2 \text{ pc}} \right)^{-1/2} \left( \frac{h/R_D}{0.3} \right)^{1/4} \text{ K}. \quad (17)$$

The emitted flux is  $F_{\text{IR}} \approx \sigma_B T^4 \min(\tau_{\text{IR}}, 1)$ . Equating  $F_*$  with  $F_{\text{IR}}$ , we find

$$T = T_{e,*} \min(\tau_{\text{IR}}, 1)^{-1/4} \text{ K}. \quad (18)$$

Note that in the optically thick case, external irradiation generates a midplane temperature,  $T$ , that is independent of optical depth. At such low temperatures (tens of K), the main source of opacity is dust, for which

$$\kappa_{\text{IR}} = 5.5 \left( \frac{T}{166 \text{ K}} \right)^2 \text{ cm}^2 \text{ g}^{-1} \quad T < 166 \text{ K} \quad (19)$$

<sup>6</sup> Gas and dust are thermally well coupled by gas-dust collisions. A  $\sim 0.1 \mu\text{m}$  grain equilibrates with surrounding gas in  $\sim 10^6$  s at the gas densities  $n \sim 8 \times 10^8 \text{ cm}^{-3}$  and temperatures  $T \sim 30$  K characterizing  $Q \sim 1$  disks.

(Bell & Lin 1994; Thompson, Quataert, & Murray 2005). The disk builds up sufficient mass to fragment when  $Q \sim 1$ , which implies

$$\frac{M_{\text{gas, crit}}}{M_{\text{BH}}} \sim \frac{c_s}{v_{\text{orb}}}. \quad (20)$$

At this time, the disk may be optically thin or thick.

We first consider the optically thin case. Combining equations (18), (19), and (20), and using  $\Sigma_g = M_{\text{gas, crit}}/\pi R^2$  for a gas disk with radius  $R$ , we find

$$M_{\text{gas, crit}} \sim 5 \times 10^4 \left( \frac{M_{\text{BH}}}{10^8 M_\odot} \right)^{6/13} \left( \frac{R}{1 \text{ pc}} \right)^{8/13} \left( \frac{T_{e,*}}{20 \text{ K}} \right)^{4/13} M_\odot. \quad (21)$$

From equation (18), the corresponding temperature is

$$T \sim 30 \left( \frac{M_{\text{BH}}}{10^8 M_\odot} \right)^{-1/13} \left( \frac{R}{1 \text{ pc}} \right)^{3/13} \left( \frac{T_{e,*}}{20 \text{ K}} \right)^{8/13} \text{ K}, \quad (22)$$

and the cooling time is

$$t_{\text{cool}} \approx 6 \left( \frac{M_{\text{BH}}}{10^8 M_\odot} \right)^{5/13} \left( \frac{R}{1 \text{ pc}} \right)^{-15/13} \left( \frac{T_{e,*}}{20 \text{ K}} \right)^{-40/13} \text{ yrs}. \quad (23)$$

The cooling condition (eq.[14]) is satisfied for  $R \gtrsim R_{\text{cool, thin}}$  where

$$R_{\text{cool, thin}} \approx 0.1 \left( \frac{M_{\text{BH}}}{10^8 M_\odot} \right)^{23/69} \left( \frac{T_{e,*}}{20 \text{ K}} \right)^{-80/69} \text{ pc}. \quad (24)$$

Once the critical gas mass is reached (eq.[21]) (for  $R \gtrsim R_{\text{cool, thin}}$ ), the disk fragments and forms stars.

For larger gas masses, the disk becomes optically thick. Using equations (19) and (20), we find that the gas mass where the optically thin to thick transition occurs is

$$M_{\text{gas, } \tau=1} \approx 6 \times 10^4 \left( \frac{R}{1 \text{ pc}} \right)^{4/5} \left( \frac{M_{\text{BH}}}{10^8 M_\odot} \right)^{-2/5} M_\odot. \quad (25)$$

For an optically thick disk, the critical mass for fragmentation is

$$M_{\text{gas, crit}} \sim 3 \times 10^4 \left( \frac{M_{\text{BH}}}{10^8 M_\odot} \right)^{1/2} \left( \frac{R}{0.3 \text{ pc}} \right)^{1/2} \left( \frac{T_{e,*}}{20 \text{ K}} \right)^{1/2} M_\odot, \quad (26)$$

where the corresponding temperature  $T = T_{e,*}$ . Note we rescaled  $T_{e,*}$  so that the disk is self-consistently optically thick. The cooling time is

$$t_{\text{cool}} \approx 100 \left( \frac{R}{0.3 \text{ pc}} \right)^{-3} \left( \frac{M_{\text{BH}}}{10^8 M_\odot} \right) \text{ yrs}. \quad (27)$$

For optically thick cooling in the regime where  $\kappa \propto T^2$ , the cooling time is independent of the gas mass. In this case, the cooling condition (eq.[14]) is satisfied for  $R \gtrsim R_{\text{cool, thick}} = 0.2(M_{\text{BH}}/10^8 M_\odot)^{-1/3}$  pc.

If a disk reaches  $Q \sim 1$ , but the cooling condition (eq.[14]) is not satisfied, then it cannot fragment immediately. Instead, gravitoturbulence heats the disk to maintain a temperature of

$$T \approx 30 \left( \frac{R}{1 \text{ pc}} \right)^{-1} \left( \frac{M_{\text{gas}}}{5 \times 10^4 M_\odot} \right)^2 \left( \frac{M_{\text{BH}}}{10^8 M_\odot} \right)^{-1} \text{ K} \quad (28)$$

so as to keep  $Q \sim 1$ . To fragment, the disk must accumulate additional mass until  $\Omega t_{\text{cool}} \lesssim 3$ . Again this cooling may proceed via optically thin or thick emission. The critical mass for fragmentation for an optically thin disk is

$$M_{\text{gas, crit}} \approx 3 \times 10^4 \left( \frac{M_{\text{BH}}}{10^8 M_{\odot}} \right)^{11/20} \left( \frac{R}{1 \text{ pc}} \right)^{7/20} M_{\odot}. \quad (29)$$

For  $R < R_{\text{cool, thick}}$ , optically thick cooling in the  $\kappa \propto T^2$  regime is too slow for the disk to fragment. Instead, the gas mass there will build up and gravitoturbulence will heat the disk until  $\kappa$  is no longer proportional to  $T^2$ , i.e.,  $T > 166 \text{ K}$ . Above this temperature,  $\kappa \approx 5.5 \text{ cm}^2 \text{ g}^{-1}$  is roughly independent of temperature (c.f. Thompson et al. 2005), though it varies by factors of a few between  $T \sim 100 - 1000 \text{ K}$ , where the upper bound is set by the dust sublimation temperature. Assuming a constant opacity, we find the critical gas mass for fragmentation to be

$$M_{\text{gas, crit}} \approx 5 \times 10^4 \left( \frac{M_{\text{BH}}}{10^8 M_{\odot}} \right)^{7/8} \left( \frac{R}{0.2 \text{ pc}} \right)^{-5/8} M_{\odot}, \quad (30)$$

for  $R < R_{\text{cool, thick}}$ .

We summarize the above results in Figure 7. We use the opacity table compiled by Semenov et al. (2003) and numerically compute the self-consistent fragmentation mass (eqns.[13] and [14]) with radiative cooling (eq.[15]), allowing for starlight (eq.[18]) and gravitoturbulent heating (eq.[28]), whichever is greater. Figure 7 shows the critical disk mass for gravitational collapse as a function of  $R$  at  $T_{e,*} = 5, 20, \text{ and } 50 \text{ K}$ . We also show the  $R^{8/13}$  scaling from equation (21), the  $R^{1/2}$  scaling from equation (26), and the  $R^{7/20}$  scaling from equation (29) in their respective regimes. We find that at  $R \approx 1 \text{ pc}$ , external irradiation dominates. For  $R \lesssim R_{\text{cool, thick}} \approx 0.2 \text{ pc}$ , gravitoturbulence heats the central disk temperature above which the opacity law,  $\kappa \propto T^2$ , no longer holds. However, we do not recover the scaling suggested by equation (30) as the opacity is not a constant above 166 K, but rather varies by factors of a few.

We have shown that depending on whether disks are externally heated (eq. [21]) or internally heated (eq. [29]), the fragmentation mass is  $3 - 5 \times 10^4 M_{\odot}$ . Gas from stellar mass loss at  $r > R_t$  is driven to  $r \approx R_t$  on a timescale  $t_{\text{flow}} \sim 10^6 \text{ yrs}$  (§2). For mass supply rates of  $\dot{M}_* \sim 10^{-4} M_{\odot} \text{ yr}^{-1}$ , the steady-state disk mass outside  $R_t$  is expected to be  $\sim 100 M_{\odot}$ , well below that required to fragment. Thus all of the gas is driven to  $R \approx R_t \sim 1 \text{ pc}$ , where it collects in a ring. The timescale for gas to viscously spread once it accumulates at  $R_t$  is

$$t_{\text{visc}} = \frac{t_{\text{dyn}}}{\alpha} \left( \frac{h}{R_t} \right)^{-2} \approx 5000 \alpha^{-1} \left( \frac{M_{\text{BH}}}{10^8 M_{\odot}} \right)^{1/2} \left( \frac{R_t}{1 \text{ pc}} \right)^{1/2} \left( \frac{T}{30 \text{ K}} \right)^{-1} \text{ Myrs}, \quad (31)$$

where  $\alpha < 1$  is the dimensionless viscosity. We compare this to the time needed to accumulate a gravitationally unstable disk,  $t_{\text{accum}} = M_{\text{gas, crit}} / \dot{M}_*$ . The mass loss rate varies as the stellar population ages. Using Starburst99, we find that as a  $2 \times 10^7 M_{\odot}$  stellar cluster ages from

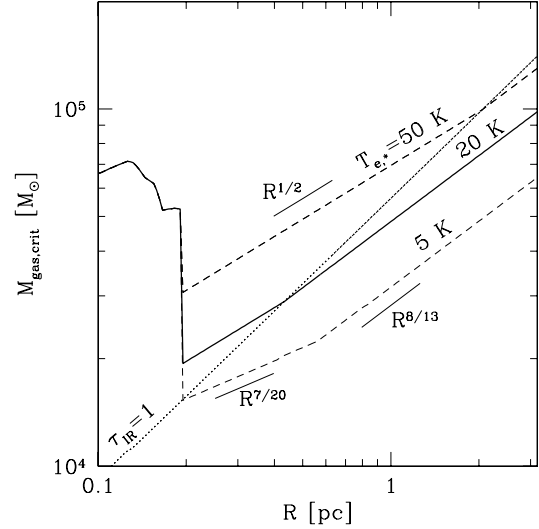


FIG. 7.— Critical gas mass for fragmentation as a function of disk radius  $R$  at  $T_{e,*} = 5$  (lower dashed line), 20 (thick solid line), and 50 K (upper dashed line) for  $M_{\text{BH}} = 10^8 M_{\odot}$ . At  $R \lesssim 0.2 \text{ pc}$ , local accretion heating dominates, while at larger radii, irradiation dominates. The dotted line shows the disk mass at which  $\tau_{\text{IR}} = 1$ . We also show the  $R^{8/13}$  scaling from equation (21), the  $R^{1/2}$  scaling from equation (26), and the  $R^{7/20}$  scaling from equation (29).

$3 \times 10^9$  to  $10^{10}$  yrs, the mass loss rate,  $\dot{M}_*$ , ranges from  $3 \times 10^{-4}$  to  $3 \times 10^{-5} M_{\odot} \text{ yr}^{-1}$ . The range in  $\dot{M}_*$  and the range in  $M_{\text{gas, crit}}$  yield  $t_{\text{accum}} \approx 100 - 2000 \text{ Myrs}$ . Hence the ratio

$$\frac{t_{\text{accum}}}{t_{\text{visc}}} \approx 0.1 \alpha \left( \frac{\dot{M}_*}{10^{-4} M_{\odot} \text{ yr}^{-1}} \right)^{-1} \left( \frac{T}{30 \text{ K}} \right)^{3/2}, \quad (32)$$

where we have used the critical mass for  $Q \sim 1$  from equation (20). Thus, even for  $\alpha \sim 1$ , the ratio  $t_{\text{accum}}/t_{\text{visc}} \lesssim 0.3$ , which implies that gas fragments at  $\sim R_t$  before accreting.

The current mass in stars in P3 is estimated to be  $\approx 4200 M_{\odot}$  (B05). The disk mass required for gravitational instability is  $\sim 6 - 10$  times higher than this (Fig. 7). Such a difference suggests a star formation efficiency  $\sim 10 - 20\%$ . A larger star formation efficiency can be accommodated if the initial mass function (IMF) of stars in this extreme environment is top heavy, which would help reconcile our estimated  $M_{\text{gas, crit}}$  with the current inferred mass of P3. There is theoretical (Nayakshin 2006; Levin 2007) and observational (Nayakshin & Sunyaev 2005; Paumard et al. 2006) evidence for a top heavy IMF in the GC starburst.

Because  $t_{\text{dyn}} \ll t_{\text{accum}}$ , it is also possible that only a small fraction of the gas fragments into stars once the disk mass exceeds  $M_{\text{gas, crit}}$ , leaving behind a stable disk with a mass only modestly below  $M_{\text{gas, crit}}$ . The excess gas would remain in the nuclear region, given the severe difficulty that stellar winds and supernovae would have in removing it from so deep in the gravitational potential of the black hole. In this case, the gas disk in the nucleus of M31 would maintain a mass of  $\sim M_{\text{gas, crit}}$ .

Since the starburst that produced P3 occurred, we expect  $\dot{M}_* \times 200 \text{ Myr} \sim 10^4 M_{\odot}$  of gas to have accumulated

near  $R_t \sim 1$  pc from ongoing stellar mass loss. This molecular gas would be analogous to the circumnuclear disk (CND) in the GC, with temperatures of  $T \approx 30$  K and extremely high densities of  $n \sim 10^9 \text{ cm}^{-3}$  ( $Q \gtrsim 1$ ). This gas would be bright in CO and HCN; the CO (1-0) flux would be  $\approx 2$  mJy (for an optically thick line).

#### 4. DISCUSSION AND CONCLUSIONS

We have argued that the origin of the young stars in P3 in M31 is rooted in the P1/P2 disk. The non-axisymmetric component of the potential from the P1/P2 disk restricts non-intersecting gas orbits to distances  $r \lesssim R_t \sim 1$  pc from the central SMBH if the pattern speed (i.e., precession frequency) of the P1/P2 disk is  $\Omega_p \lesssim 3 - 10 \text{ km s}^{-1} \text{ pc}^{-1}$ . At larger radii, gas finds itself in intersecting orbits; it shocks, loses energy, and gets driven to  $R_t \sim 1$  pc. This is comparable to the maximum radial extent of the A stars of P3.

Stellar mass loss from the P1/P2 disk can supply the gas that formed P3. Stellar winds supply mass at a rate of  $\sim 10^{-4} M_\odot \text{ yr}^{-1}$  for a  $\sim 10^{10}$  yr old population. This gas accumulates in a disk at  $r \lesssim R_t$ . The conditions for fragmentation (eqns. [13] and [14]) give a critical gas mass of  $\sim 5 \times 10^4 M_\odot$ . Hence, every  $\sim 500$  Myr, the disk accumulates enough mass to fragment and produces a starburst. This recurrence time is consistent with the age of the A stars of 200 Myr (B05). In addition, the observed alignment of the P3 disk with the P1/P2 disk is consistent with our argument that the P1/P2 disk supplies the gas which formed P3.

Several predictions arise naturally out of this model. First, the pattern speed of the eccentric stellar disk should be  $\Omega_p \lesssim 3 - 10 \text{ km s}^{-1} \text{ pc}^{-1}$ . Current observational constraints on the pattern speed are weak (see Appendix A). Second, there should be  $\sim 10^4 M_\odot$  of gas in the nucleus of M31 from accumulation of gas since the last starburst that produced P3. This molecular gas would be analogous to the CND at the GC. Such gas would have a temperature of  $\sim 30$  K, be at extremely high densities  $n \sim 10^9 \text{ cm}^{-3}$ , and be bright in CO and HCN with a CO (1-0) flux of  $\approx 2$  mJy and a line width of  $\approx 1000 \text{ km s}^{-1}$ . Under these conditions, dust will emit with a flux of  $\sim 20$  mJy at  $70 \mu\text{m}$ ,  $\sim 100$  mJy at  $160 \mu\text{m}$ , and  $\sim 0.1$  mJy at 1 mm. Finally, starbursts at  $\lesssim 1$  pc in M31 should occur every  $10^8 - 10^9$  yrs. These older generations of stars and stellar remnants may be detectable.

Observations indicate that P3 appears to be a circular disk around the SMBH. Gas orbits around the SMBH are eccentric in the presence of the P1/P2 disk as illustrated in Figure 1. However, stars that form from an eccentric gas disk may not have an eccentric distribution themselves at later times. Once the  $Q \sim 1$  gas disk turns into stars, these stars will precess differentially because of their own self-gravity. We estimate the differential precession rate to be

$$\frac{d\dot{\omega}}{dR} \Delta R \sim \Omega \left( \frac{M_{\text{P3}}}{M_{\text{BH}}} \right) \left( \frac{\Delta R}{R} \right) \quad (33)$$

where  $\dot{\omega}$  is the precession frequency of a star at radius  $R$ , and  $\Delta R$  is the initial radial extent of the P3 stellar disk with mass  $M_{\text{P3}}$ . A spread of  $\Delta R/R \sim 0.1$  in the orbits of the P3 stars can be generated by viscous spreading of the deposited gas prior to star formation. Taking  $M_{\text{P3}}/M_{\text{BH}} \sim 10^{-4}$ , we find that stars in P3 differentially precess out of their initially apsidally aligned structure over a timescale  $10^5 \Omega^{-1} \sim 10^8$  years, comparable to the age of the A stars.

Our model may be applicable to other galaxies with double nuclei in addition to M31. Lauer et al. (1996) observed a double nucleus in NGC 4486B with a 12 pc separation. Debattista et al. (2006) detected a double nucleus in VCC 128 with a 32 pc separation. Thatte et al. (2000) also detected a double nucleus in the starburst galaxy M83 with a 5.4 pc separation. If these double nuclei are associated with non-axisymmetric stellar distributions, very compact nuclear starbursts and dense nuclear molecular gas may be common features of galactic nuclei.

Finally, we briefly discuss our model in the context of the GC. Observations suggest that the  $1.3 \times 10^4 M_\odot$  of young massive stars in the GC are concentrated between  $r \sim 0.04 - 0.4$  pc (Ghez et al. 2005; Paumard et al. 2006), similar in mass and radial extent to M31. A non-axisymmetric component of the potential may explain the radial extent of these young stars, which otherwise can only be accounted for by the assumption that gas is supplied on very low angular momentum orbits. If the non-axisymmetric component were due to an eccentric disk of old stars, it would likely remain undetected because of extinction.

We thank R. Genzel, A. Loeb, B. Paczynski, L. Strubbe, and S. Tremaine for useful discussions. We thank L. Blitz and A. Bolatto for useful discussions and performing CO observations on M31. We thank B. Johnson for presenting a talk on M31 in the Astro Reading Group (ARG) that led to this project. We also thank G. Bower, G. Howes, B. Metzger, and B. Schmelkel for leading other seminars in the ARG. We would also like to acknowledge all ARG participants. P.C. thanks the Institute for Advanced Study and the Canadian Institute for Theoretical Astrophysics for their hospitality. P.C. is supported by the Miller Institute for Basic Research. R.M.-C. is supported by a NSF graduate fellowship. E.C. is supported in part by an Alfred P. Sloan Fellowship and NSF-AST grant 0507805. E.Q. was supported in part by NASA grant NNG05GO22H and the David and Lucile Packard Foundation.

#### APPENDIX

##### DYNAMICS OF P1 AND P2

The most widely accepted model for the double nucleus of M31 is that of an eccentric stellar disk (T95). T95 fits the light distribution with three apsidally aligned ellipses with the SMBH at one focus. Stars on these elliptical Keplerian

TABLE A1. MODEL PARAMETERS FROM PEIRIS &amp; TREMAINE (2003).

Parameter	Aligned Model	Unaligned Model
$\alpha$	0.288	0.197
$a_e$ [pc]	3.97	4.45
$a_g$ [pc]	1.51	1.71
$w$ [pc]	1.53	1.52
$a_0$ [pc]	4.61	1.37
$c_2$ [pc]	3.79	4.24

orbits pile up at apoapse, giving rise to P1. A suitable nesting of orbits gives rise to P2 at periapse. PT03 performed a more careful calculation to fit the light and velocity distributions, using Keplerian ellipses again. These models do not take disk self-gravity into account. Since the stellar disk mass is nearly  $2 \times 10^7 M_\odot$ , comparable to the SMBH mass of  $\sim 10^8 M_\odot$  (B05), disk self-gravity has significant effects on the dynamics of both stars and gas.

Other workers have developed self-consistent models for the dynamics of such an eccentric stellar disk. Statler (1999) created self-consistent models for a stellar disk assuming that stars follow periodic orbits. This work was expanded by Salow & Statler (2004), who find high pattern speeds  $\Omega_p \sim 30 \text{ km s}^{-1} \text{ pc}^{-1}$ . Sambhus & Sridhar (2002) used families of prograde and retrograde loop orbits to fit the light distribution and found  $\Omega_p \approx 16 \text{ km s}^{-1}$ . Bacon et al. (2001) showed through N-body simulations that the  $m = 1$  perturbation can be long-lived,  $\sim 100$  Myrs for low pattern speeds  $\Omega_p \lesssim 3 \text{ km s}^{-1} \text{ pc}^{-1}$ . Finally, Sambhus & Sridhar (2000) utilized a variant of the Tremaine-Weinberg method (Tremaine & Weinberg 1984) to obtain an observational constraint on the pattern speed of  $< 30 \text{ km s}^{-1} \text{ pc}^{-1}$  (for a disk inclination relative to the sky plane of 77 degrees).

As the constraints on the pattern speed are weak, we have elected to take PT03's fits to the P1/P2 disk and to experiment with a range of values of  $\Omega_p$ . We use their formulae for the disk eccentricity profile and surface density (their eqs.[12] and [17]):

$$e_m(a) = \alpha (a_e - a) \exp \left[ -\frac{(a - a_g)^2}{2w^2} \right], \quad (\text{A1})$$

$$\Sigma(a) = \Sigma_0 \frac{a^2 \exp(-a/a_0)}{1 + \exp[4(a - c_2)]}, \quad (\text{A2})$$

where  $a$  is the semi-major axis in pc,  $e_m$  is the mean eccentricity, and the effective surface density,  $\Sigma(a)$ , is defined as  $dM = 2\pi a \Sigma(a) da$ , where  $dM$  is the mass between  $a$  and  $a + da$ . We take the maximum semi-major axis to be  $a = 8$  pc. The normalization  $\Sigma_0$  is set by  $M_D/M_{\text{BH}}$ , which we vary. For convenience we list the fitting parameters (their Table 2) in our Table 1. We focus on PT03's nonaligned model in this paper, but we have studied their aligned model as well. In the aligned model, for  $R_t \lesssim 1$  pc, we find the required pattern speed is  $\Omega_p \lesssim 6 \text{ km s}^{-1} \text{ pc}^{-1}$  for  $M_D/M_{\text{BH}} = 0.1$  and  $M_{\text{BH}} = 10^8 M_\odot$  for the softening length of  $h = 0.1$  pc, similar to the nonaligned model.

## REFERENCES

- Bacon, R., Emsellem, E., Combes, F., Copin, Y., Monnet, G., & Martin, P. 2001, A&A, 371, 409  
Bell, K. R. & Lin, D. N. C. 1994, ApJ, 427, 987  
Bender, R., Kormendy, J., Bower, G., Green, R., Thomas, J., Danks, A. C., Gull, T., Hutchings, J. B., Joseph, C. L., Kaiser, M. E., Lauer, T. R., Nelson, C. H., Richstone, D., Weistrop, D., & Woodgate, B. 2005, ApJ, 631, 280 (B05)  
Binney, J. & Tremaine, S. 1987, *Galactic Dynamics*, (Princeton: Princeton University Press)  
Debattista, V. P., Ferreras, I., Pasquali, A., Seth, A., De Rijcke, S., & Morelli, L. 2006, ApJ, 651, L97  
Draine, B. T. 2003, ARA&A, 41, 241  
Gammie, C. F. 2001, ApJ, 553, 174  
Ghez, A. M., Salim, S., Hornstein, S. D., Tanner, A., Lu, J. R., Morris, M., Becklin, E. E., & Duchne, G. 2005, ApJ, 620, 744  
Ichikawa, S. & Osaki, Y. 1994, PASJ, 46, 621  
King, I. R., Stanford, S. A., & Crane, P. 1995, AJ, 109, 164  
Kormendy, J. & Bender, R. 1999, ApJ, 522, 772  
Lamers, H. J. G. L. M. & Cassinelli, J. P. 1999, *Introduction to Stellar Winds*, (Cambridge: Cambridge University Press)  
Lauer, T. R., Faber, S. M., Groth, E. J., Shaya, E. J., Campbell, B., Code, A., Currie, D. G., Baum, W. A., Ewald, S. P., Hester, J. J., Holtzman, J. A., Kristian, J., Light, R. M., Ligynds, C. R., O'Neil, E. J., Jr., & Westphal, J. A. 1993, AJ, 106, L1436  
Lauer, T. R., Tremaine, S., Ajhar, E. A., Bender, R., Dressler, A., Faber, S. M., Gebhardt, K., Grillmair, C. J., Kormendy, J., & Richstone, D. 1996, ApJ, 471, L79  
Levin, Y. 2007, MNRAS, 374, 515  
Leitherer, C., Schaerer, D., Goldader, J. D., Delgado, R. M. G., Robert, C., Kune, D. F., de Mello, D. F., Devost, D., & Heckman, T. M. 1999, ApJS, 123, 3  
Light, E. S., Danielson, R. E., & Schwarzschild, M. 1974, ApJ, 194, L257  
Menou, K. Narayan, R., & Lasota, J-P., 1999, ApJ, 513, 811  
Nayakshin, S. 2006, MNRAS, 372, 143  
Nayakshin, S. & Sunyaev, R. 2005, MNRAS, 364, 23  
Nieto, J.-L., Macchetto, F. D., Perryman, M. A. C., di Serego Alighieri, S., & Lelievre, G. 1986, A&A, 165, 189  
Paczynski, B. 1977, ApJ, 216, 822  
Papaloizou, J. & Pringle, J. E. 1977, MNRAS, 181, 441  
Peiris, H. V. & Tremaine, S. 2003, ApJ, 599, 237 (PT03)  
Paumard, T., Genzel, R., Martins, F., Nayakshin, S., Beloborodov, A. M., Levin, Y., Trippe, S., Eisenhauer, F., Ott, T., Gillessen, S., Abuter, R., Cuadra, J., Alexander, T., Sternberg, A. 2006, ApJ, 643, 1011  
Salow, R. M. & Statler, T. S. 2001, ApJ, 551, L49  
Salow, R. M. & Statler, T. S. 2004, ApJ, 611, 245  
Sambhus, N. & Sridhar, S. 2000, ApJ, 539, L17  
Sambhus, N. & Sridhar, S. 2002, A&A, 388, 766  
Semenov, D., Henning, T., Helling, C. Ilgner, M., & Sedlmayr, E. 2003, A&A, 410, 611  
Shlosman, I., Frank, J., Begelman, M. C. 1989, Nature, 338, 45  
Shlosman, I. & Begelman, M. C. 1989, ApJ, 341, 685  
Statler, T. S. 1999, ApJ, 524, L97

Thatte, N., Tecza, M., & Genzel, R. 2000, A&A, 364, L47

Thompson, T.A., Quataert, E., & Murray, N. 2005, ApJ, 630, 167

Tremaine, S. & Weinberg, M. D. 1984, ApJ, 282, L5

Tremaine, S. 1995, AJ, 110, 628 (T95)

Vazquez, G. A. & Leitherer, C. 2005, ApJ, 621, 695